Random Plasmonic Laser Based on Bismuth/Aluminum/Yttria/ Silver Co-Doped Silica Fiber with Microcavity Shaped Tip

J. A. de la Fuente-León , M. A. Martinez Gámez * , J. L. Lucio M. , A. V. Kir'yanov , K. G. Hernández-Chahín , M. C. Paul

Posted Date: 7 October 2024

doi: 10.20944/preprints202410.0458.v1

Keywords: random fiber laser; bismuth; nanoparticles; surface plasmon resonance

 doi:10.20944/preprints202410.0458.v1

Article

Random Plasmonic Laser Based on Bismuth/Aluminum/Yttria/ Silver Co-Doped Silica Fiber with Microcavity Shaped Tip

J. A. de la Fuente-León [1], M. A. Martinez Gámez [1,*], J. L. Lucio M. [2], A. V. Kir'yanov [1], K. G. Hernández-Chahín [2] and M. C. Paul [3]

[1] Centro de Investigaciones en Óptica, Loma del Bosque 115, Col. Lomas del Campestre, León, Gto., México
[2] Laboratorio de Aplicaciones Cuánticas, División de Ciencias e Ingenierías del Campus León de la Universidad de Guanajuato. Loma del Bosque 103, Col. Lomas del Campestre, León, Gto., México
[3] Fiber Optics and Photonic Division, Central Glass and Ceramic Research Institute, 196, Raja S.C. Mullick Road, Kolkata-700 032, India
* Correspondence: mamg@cio.mx

Abstract: In this study, we demonstrate a proof of principle of an all-fiber random laser due to the plasmonic effect. This was achieved in a fiber co-doped with Bismuth/Aluminum/Yttria/Silver in which a microsphere (microcavity) at the fiber's tip was made using a splicing machine. The presence in the fiber of Bismuth- and silver nanoparticles along with Bismuth-Aluminum phototropic centers stands behind the observed phenomenon. The effect can be attributed to in-pair functioning of this unit as an active medium and volumetric plasmonic feedback, with the result being lasing at 807 nm under 532-nm pumping with notably low (~2 mW) threshold.

Keywords: random fiber laser; bismuth; nanoparticles; surface plasmon resonance

1. Introduction

Since their first demonstration in 1994 by Lawandy *et al.* [1] and De Matos *et al.* [2], interest to random lasers (RL) and particularly to random fiber lasers (RFL) has increased considerably. The happened was mostly due to the identification of materials with properties that have potential for making RL/RFL, such as conjugated polymer films [3], laser dye molecules [4], organic dye doped gel films [5,6], dielectric materials [7–10] and metallic nanoparticles (NP). RL/RFL offer such advantages as low cost, simplicity of fabrication, and potential applicability in versatile areas, e.g., in optical engineering [11–13], biomedical diagnostics [14], lighting technologies [15], optical astronomy and microscopy [8,16], etc. Meanwhile, the major challenges for these devices are pump threshold reduction and possible miniaturization. The reader can refer to a recent review of the state-of-the-art of RFL [17].

The gain in RL/RFL is produced within an active medium that is basically featured by high scattering, caused by NP. In this sense, the use of metal NP, e.g., Bismuth (Bi) NP, has become relevant in the field as such metallic inclusions exhibit optical properties different from those exhibited by bulk materials [18,19]. It is known that if electromagnetic radiation at proper wavelength is incident on metallic NP, this gives rise to the localized surface plasmon resonance (SPR) [20], which in turn leads to strong light scattering, resonant optical absorption, and increment of electric field strength in the vicinity of NP surface.

Meanwhile, on the one hand, over the past few years, the use of Bi-doped fibers (BDF) towards the development of amplifiers and lasers on their base has shown significant progress. However, most of the research with BDF was focused on getting gain/lasing in the 'windows' in the near-infrared (NIR) region, uncoverable with fibers doped with rare-earths but easily accessible with BDF due to Bi active centers (BAC) inherent in them (see e.g., [21–24]). On the other hand, in a few reports

 doi:10.20944/preprints202410.0458.v1

[25–30] it was revealed that co-doping of glasses with rare earths and silver (Ag) NP can improve the fluorescence potential of the former. The ground behind the effect is the overlap of the Ag-NP SPR's peaks with the absorption or fluorescence bands of the rare-earth ions (see e.g., [31–35]).

Bearing the said in mind, we attempted (and were successful) in fabricating silica fiber co-doped with Bi and Ag (hereafter – 'BAYAg fiber') with an aim to explore a similar effect to the one referred to, i.e., to examine a combinative potential of BAC (for lasing) and Bi-NP/Ag-NP (to enroll SPR). To the best of our knowledge, this is done for the first time. Furthermore, we also report below (as well for the first time), a design and clue characteristics of a RL based on the plasmonic effect using this fiber. Namely, we managed the fiber to bear on-tip a specially prepared microsphere (microcavity). The idea behind the design was to take the unique advantage that it provides, viz., a combination of the pronounced fluorescence in the visible (VIS) range at a properly chosen pump wavelength (given the presence of BAC with characteristic spectral bands) and the SPR phenomenon (given the presence of Bi-NP/Ag-NP); one more advantage of the fiber is its low loss from in VIS/NIR. As a result, we present a small-size, low-threshold, 807-nm (under 532-nm pumping) RFL, never reported before. Note that the described approach offers a roadmap to manufacture similar RFL in a very simple way.

2. Materials and Methods

We used for experiments BAYAg (Bi/Al/Y/Ag co-doped) optical fiber to implement the device we shall report below. The raw chemical materials utilized to fabricate it are as follows:

$$1.5(M)Al(NO_3)_3 + 0.5(M)AgNO_3 + 0.1(M)Bi(NO_3)_3 + 0.2(M)Y(NO_3), \quad (1)$$

where M stands for moles.

The fiber's core diameter and N.A. are 12.6 μm and 0.19, respectively. The fiber is strongly multimode within the entire VIS-NIR range as its cutoff wavelength is ~3.14 μm. Its absorption and fluorescence spectra (at ~10-mW excitation using a fibered laser diode (LD) emitting at 406 nm) for two lengths are shown in Figure 1a,b, respectively; the cross-sectional image of the fiber at white-light illumination is added in the inset to Figure 1a. One can reveal from the spectra that there are the contributions in the fiber's absorption/fluorescence stemming from doping with Bi (Bi^0 or/and its agglomerates, e.g., NP, and Bi-Al BAC (see e.g., [24,36,37]) and Ag (presumably in the form of Ag-NP) (see e.g., [19]).

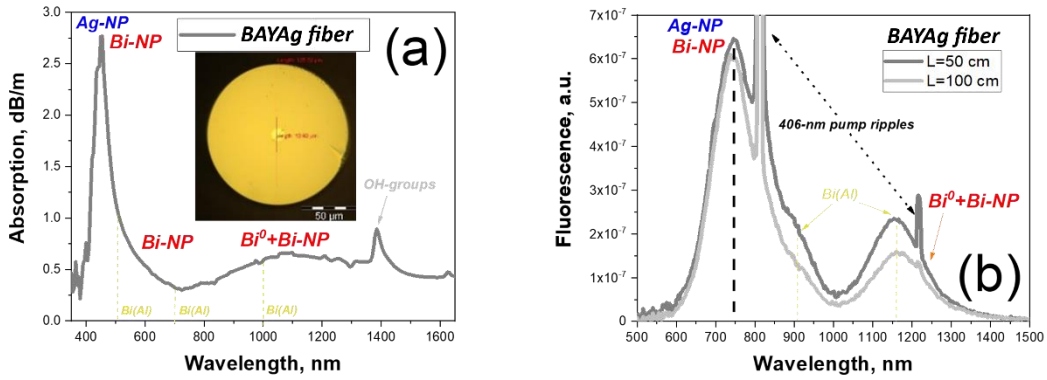

Figure 1. (a) Absorption and (b) fluorescence spectra of BAYAg fiber, employed in the following experiments. Inset in (a) – microphotograph of its cleaved end at WL illumination.

In Figure 2a, we report the X-ray energy dispersive spectroscopy (EDS) of the fiber, which was obtained using a scanning electron microscope (Jeol model JSM-7800F). The result shows the presence of Bi, Ag, O, Al and Si species in the fiber's core-area. Note that the mostly pronounced peaks corresponding to Bi and Ag are grouped in Figure 2a at ~2.3 to ~3.4 keV, so it is natural to consider that their sources are NP comprising both Bi and Ag species. Furthermore, since the core of the fiber was fabricated using the composition (1) at a high temperature (~2000°C), the start Ag/Bi-containing compounds 0.5(M) $AgNO_3$ + 0.1(M) $Bi(NO_3)_3$ should fade during the fabrication, leading to the

 doi:10.20944/preprints202410.0458.v1

following two basic effects: *a*) the thermal decomposition of $AgNO_3$ and $Bi(NO_3)_3$ according to the reactions: $2AgNO_3 \rightarrow 2Ag\text{-}NP(solid) + 2NO_2(gas) + O_2(gas)$ and $2Bi(NO_3)_3 \rightarrow 2Bi\text{-}NP(solid) + 9O_2(gas) + 3N_2(gas)$ and *b*) formation of metallic Bi^0 and/or clusters $(Bi_n)^0$ as well as Bi-NP via a redox reaction [38–42]. Thus, the final fiber is expected to contain Bi-NP, Ag-NP and probably 'hybrid' Bi/Ag-NP [18].

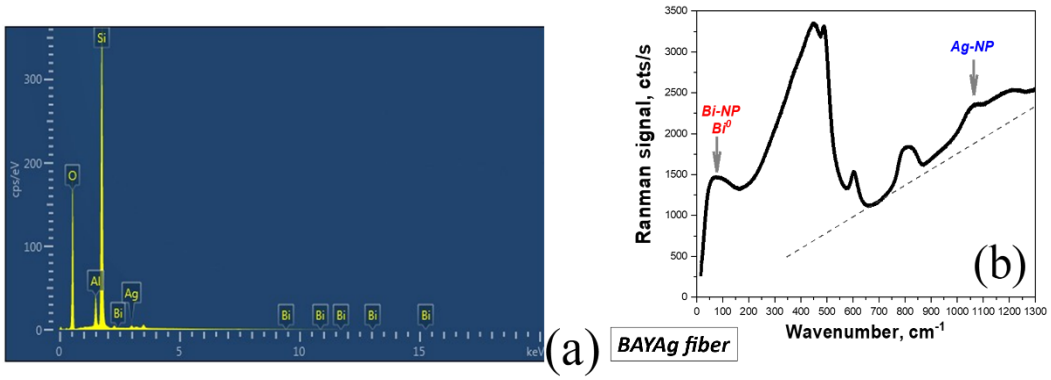

Figure 2. (a) X-ray ED spectrum for BAYAg fiber and (b) its Raman spectrum.

In Figure 2b, we present the Raman response of BAYAg fiber; it was obtained employing the standard technique adapted to optical fiber. The excitation wavelength in this case was 514 nm (i.e., close to the pump one, 532 nm, in the main-course experiments, reported below); in the experiment, we used short-focus objective (50x) launching the pump-light into the fiber. An analysis of the Raman spectrum reveals that: *a*) the fiber under study shows strong fluorescence, seen as steep rise of the detected signal at increasing wavenumber (guided to the eye by the dashed gray line), which is confirmed by our experiments on fluorescence and lasing at 532-nm pumping and *b*) the pronounced peak in the spectrum at 50…150 cm^{-1} evidences a notable contribution from the Bi-NP and Bi^0 species (both Raman-active in this domain) while the peak near 1050 cm^{-1}, also expressed, can indicate the presence of Ag-NP [18] (both features are highlighted by gray arrows in Figure 2b).

3. Results

A 10-cm long piece of the fiber was placed in a fusion splicing machine (FSM-100 Arc Master Fujikura), specially programmed for making a microsphere on a tip of one of the fiber's ends. A sketch of the machine's program, utilized for making a microsphere-on-fiber-tip unit, is demonstrated in Figure 3.

The resulting component can be addressed as a nearly spherical (slightly elliptical) cavity with a radius of ~300 μm. In Figure 4, we show a schematized view of our RFL based on the design described above. The light from a pump laser (a fiberized LD at "green" wavelength) is launched through splice into the fiber from the side opposite to the one where the microsphere was manufactured, so it first propagated along the entire fiber length and then within the microsphere, interacting with the dopants and igniting down-converted emission, the spectrum of which is in the orange-yellow region.

Note that the emission in our case is born within the microcavity, at the farthest part where the pump light enters and is well-directional (highlighted by the arrow in Figure 3b), which could be seen by the naked eye. the outside 'lightening' of our setup when pump power is set close to the laser threshold. Thus, the microsphere in our case functions simultaneously in two ways: on the one hand, it is of adequate size to be capable to produce the energy density inside it high enough for the 3D-plasmonic feedback mechanism to occur and, on the other hand, the tip of the microcavity acts as a lens, guiding the emitted radiation along the axis of the optical fiber. As seen from Figure 3c, the green light (at 532 nm) comes from the pumping LD and the orange light is born in the fiber, to be presumably produced by the combined fluorescence of Ag-NP and Bi(Al) BAC (see Figure 1b).

Preprints.org (www.preprints.org) | NOT PEER-REVIEWED | Posted: 7 October 2024 doi:10.20944/preprints202410.0458.v1

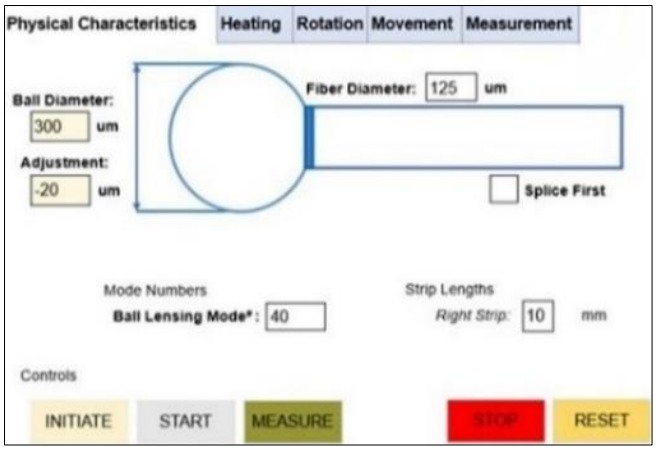

Figure 3. Programming a make-up of microsphere-on-fiber-tip structure using FSM.

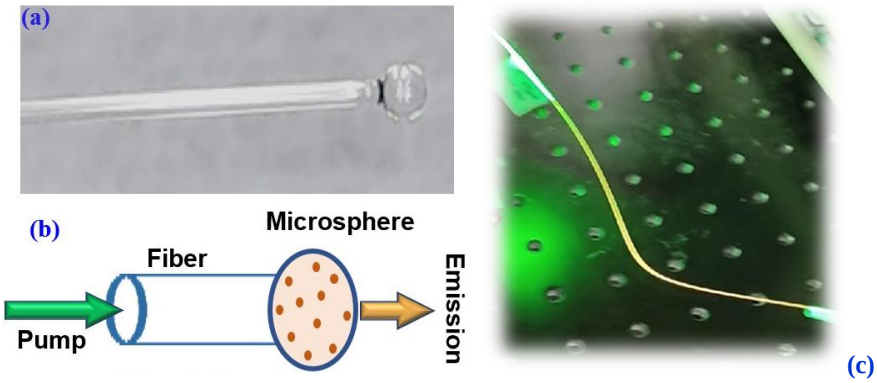

Figure 4. (a) Lateral view of the optical-microscopy image of the microcavity on BAYAg fiber tip; (b) scheme of the plasmonic RFL based on microcavity-tipped BAYAg fiber; (c) fluorescence image of the fiber (without a microsphere on tip), pumped by 532-nm LD.

The measurements were performed with an Ando AQ-6312B optical spectrum analyzer, set to a spectral resolution of 0.05 nm. To examine the developed fiber-microcavity system, we pumped it using a standard fibered LD at 532 nm; launched into the BAYAg fiber pump power was limited to ~10 mW. The results are demonstrated in Figures 5–7.

Figure 5 shows the spectral behavior of the system at passing through laser threshold. It is clearly seen from the figure an abrupt transformation of the optical spectrum from the spectrally smooth fluorescence centered at ~730 nm (see the orange spectrum, captured at pump power of ~1 mW) to the narrow-line (~1.5 nm in FWHM) lasing at ~807 nm (see the blue spectrum, captured at pump power of ~2.0 mW). First, note the tremendously growing laser-line's amplitude after passing the threshold and simultaneously occurring depressing of the remnant broadband fluorescence on its background, which is apparent from comparison of the two spectra. This behavior appears to provide strong evidence for 'true' lasing to switch-up in the system. Second, note that the drawn effect of self-started lasing never happened when using a 'naked' BAYAg fiber (i.e., without a microsphere on its tip). Third, note that yet "under-threshold" orange fluorescence (refer to the orange curve in Figure 5) itself is spectrally narrower than the one shown in Figure 1b; this points to that it is mainly produced in the microcavity, say, in effect of whispery-modes developing inside the latter. Figure 6 demonstrates the laser spectra measured at the system output. As seen, for all 532-nm pump powers explored (up to 10 mW), the narrow-line (~1.5 nm in FWHM) light at the unchanged central wavelength (807 nm) with steadily growing (at increasing the pump) amplitude is generated. The power and the FWHM of the output laser light in function of pump power are presented in Figure 7. As seen, the behavior of output power vs. pump power (nonlinear growth) is typical for laser action; accordingly, linewidth steadily decreases at increasing pump power.

Preprints.org (www.preprints.org) | NOT PEER-REVIEWED | Posted: 7 October 2024 doi:10.20944/preprints202410.0458.v1

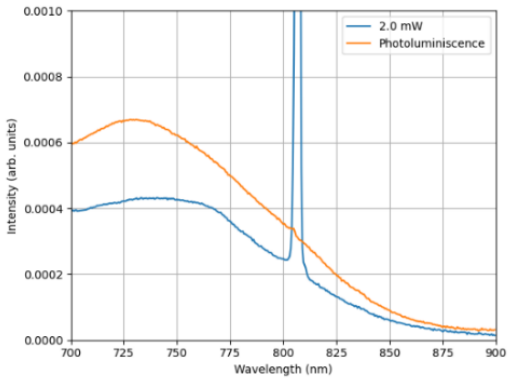

Figure 5. Transience from fluorescence (orange curve) to lasing (blue curve) around threshold.

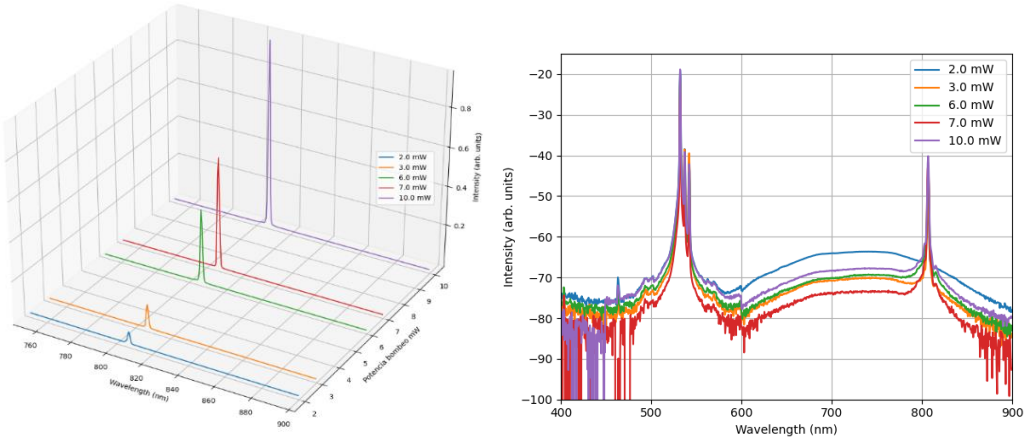

Figure 6. Plasmonic RL-emission at 807 nm: optical spectra recorded at variable pump power, launched into BAYAg fiber: on left – "3D" view of the laser line (linear scaling); on right – 'common' "2D" spectra (logarithmic scaling), extended for showing the pump-light.

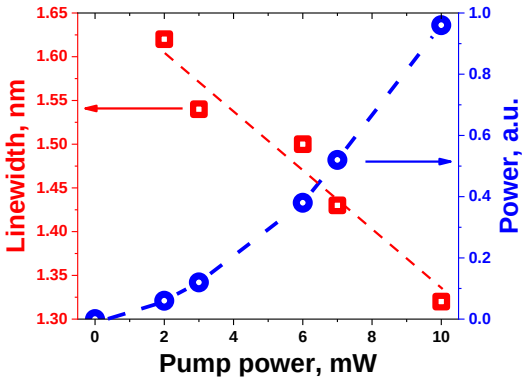

Figure 7. Power (right axis) and line FWHM (left axis): 807-nm lasing in function of 532-nm pump power.

4. Discussion

The experimental data reported above clearly reveal the achievement of laser emission mentioned in the title of our paper. A scenario with getting the results can be qualitatively explained as follows. The way we approach the phenomenon comprises, with adaptations required for the case of Bi as an emission-active species, the plasmonic effect, the energy transfer among Ag/Bi co-dopants, and the feedback of untrivial kind.

In this regard, note that different authors shared evidence that the addition of silver can lead to improvement of the luminescence properties of a material, say, based on rare earths [25–35]. A similar

 doi:10.20944/preprints202410.0458.v1

phenomenon was uncovered by C. Van der Horst et al. [19] for Bi who performed a study of the synthesis and characterization of Bi-NP/Ag-NP in glasses, which particularly reports the absorption spectrum of the material in the UV-VIS range where absorption peaks characteristic of these two kinds of NP are observed. Furthermore, it ought to remark that the plasmonic resonances of Ag-NP and Bi-NP overlap and that the resulting spectrum is such that it limits the possibility of reabsorption of the fluorescence emitted by Bi(Al) BAC (or B^0 and its agglomerates) [24,36–39].

Furthermore, regarding our current realization of the fiber-based RL, we consider that the plasmon enhances the absorption at the pump wavelength (532 nm), which has the effect of reducing the threshold power for lasing at 807 nm and enhances the field in the nearby of Bi(Al) BAC (or B^0-related species), and presumably those effects are responsible of the orange emission that ultimately results in lasing [43].

It deserves mentioning, too, is that, formally, no 'common' feedback amplification is provided in our case to generate the laser light but instead, as explained by De Matos *et al.* [2], "the optical plasmonic feedback (Bi-NP and Ag-NP) in the random laser is provided within the amplifying medium by random light paths that result in an increased emission intensity and reduced line width" which partly explains our main results. Furthermore, it is to underline the crucial role that plays the microcavity in the form of microsphere on the fiber's tip: such microcavities provide strong light confinement and scattering that ultimately lead to and facilitate RL [44].

5. Conclusions

The data reported in this paper allow the following conclusions to be made. The superposition of the SPR at Ag-NP/Bi-NP, the fluorescence spectrum of the Bi active centers, namely of Bi(Al) type, and the geometry used (viz., the microcavity on the fiber's tip, providing effective feedback), are the ground of the reported narrow-linewidth, low-threshold lasing system we are reporting. Summarizing, we have shown that *a*) Ag/Bi NP in-pair with Bi(Al) Bi active centers in the BAYAg fiber serve as the clue factors to get the random laser; *b*) the microcavity (microsphere on the fiber's tip) is a prerequisite for enrolling the high-intensity and high-directionality of outcoming laser light. Compared to others, our design of RFL, is feasible and easy to realize.

Author Contributions: Conceptualization, M.A.M.G., J.L.L.M., A.V.K., M.C.P.; methodology, M.A.M.G., J.L.L.M.; formal analysis, M.A.M.G., J.L.L.M., A.V.K., K.G.H.C.; investigation, J.A.F.L., M.A.M.G., A.V.K., K.G.H.C., M.C.P.; writing—original draft preparation, M.A.M.G., J.L.L.M., A.V.K.; writing—review and editing, M.A.M.G., A.V.K. All authors have read and agreed to the published version of the manuscript.

Conflicts of Interest: The authors declare no conflicts of interest.

References

1. Lawandy, N.M.; Balachandran R.; Gomes A.; Sauvain, E. Laser action in strongly scattering media. *Nature* 1994, **368**, 436–438.
2. de Matos, C.J.; Menezes, L.D.S.; Brito-Silva, A.M.; Martinez Gámez, M.A.; Gomes, A.S.; de Araújo, C.B. Random fiber laser. *Phys. Rev. Lett.* 2007, **99**, 153903.
3. Frolov, S.; Gellermann, W.; Ozaki, M.; Yoshino, K.; Vardeny, Z. Cooperative emission in π-conjugated polymer thin films. *Phys. Rev. Lett.* 1997, **78**, 729.
4. Dice, G.; Mujumdar, S.; Elezzabi, A. Plasmonically enhanced diffusive and subdiffusive metal nanoparticle-dye random laser. *Appl. Phys. Lett.* 2005, **86**, 131105.
5. Chang, S.-W.; Liao, W.-C.; Liao, Y.-M.; Lin, H.-I.; Lin, H.-Y.; Lin, W.-J.; Lin, S.-Y.; Perumal, P.; Haider, G.; Tai, C.-T.; Shen, K.-C.; Chang, C.-H.; Huang, Y.-F.; Lin, T.-Y.; Chen, Y.-F. A white random laser. *Sci. Reports* 2018, **8**, 1–10.
6. Parola, S.; Julián-López, B.; Carlos, L.D.; Sanchez, C. Optical properties of hybrid organic-inorganic materials and their applications. *Adv. Funct. Mater.* 2016, **26**, 6506–6544.
7. Sapienza, R. Determining random lasing action. *Nat. Rev. Phys.* 2019, **1**, 690–695.
8. Luan, F.; Gu, B.; Gomes, A.S.; Yong, K.-T.; Wen, S.; Prasad, P.N. Lasing in nanocomposite random media. *Nano Today* 2015, **10**, 168–192.
9. Cao, H. Review on latest developments in random lasers with coherent feedback. *J. Phys. A: Math. Gen.* 2005, **38**, 10497.

 doi:10.20944/preprints202410.0458.v1

10. Meng, X.; Fujita, K.; Murai, S.; Matoba, T.; Tanaka, K. Plasmonically controlled lasing resonance with metallic-dielectric core shell nanoparticles. *Nano Lett.* 2011, **11**, 1374–1378.
11. Redding, B.; Choma, M.A.; Cao, H. Speckle-free laser imaging using random laser illumination. *Nat. Photonics* 2012, **6**, 355–359.
12. Cui, L.; Shi, J.; Wang, Y.; Zheng, R.; Chen, X.; Gong, W.; Liu, D. Retrieval of contaminated information using random lasers. *Appl. Phys. Lett.* 2015, **106**, 201101.
13. Churkin, D.V.; Sugavanam, S.; Vatnik, I.D.; Wang, Z.; Podivilov, E.V.; Babin, S.A.; Rao, Y.; Turitsyn S.K. Recent advances in fundamentals and applications of random fiber lasers. *Adv. Opt. Photonics* 2015, **7**, 516–569.
14. Wang, Y.; Duan, Z.; Qiu, Z.; Zhang, P.; Wu, J.; Zhang, D.; Xiang, T. Random lasing in human tissues embedded with organic dyes for cancer diagnosis. *Sci. Reports* 2017, **7**, 1–7.
15. Ma, R.; Rao, Y.J.; Zhang, W.L.; Hu, B. Multimode random fiber laser for speckle-free imaging. *IEEE J. Sel. Top. Quantum Electron.* 2018, **25**, 1–6).
16. Mermillod-Blondin A.; Mentzel, H.; Rosenfeld, A. Time-resolved microscopy with random lasers. *Opt. Lett.* 2013, **38**, 4112–4115.
17. Han, B.; Cheng, Q.; Tao, Y.; Ma, Y.; Liang, H.; Ma, R.; Qi, Y.; Zhao, Y.; Wang, Z.; Wu H. Spectral manipulations of random fiber lasers: principles, characteristics, and applications. *Las. Photon. Rev.* 2024, **18**, 2400122.
18. Toudert, J.; Serna, R.; Jimenez de Castro, M. Exploring the optical potential of nano-bismuth: tunable surface plasmon resonances in the near ultraviolet-to-near infrared range. *J. Phys. Chem. C* 2012, **116**, 20530–20539.
19. Van der Horst, C.; Silwana, B.; Iwuoha, E.; Somerset, V. Synthesis and characterization of Bismuth-Silver nanoparticles for electrochemical sensor applications. *Anal. Lett.* 2015, **48**, 1311–1332.
20. Hutter E.; Fendler, J.H. Exploitation of localized surface plasmon resonance. *Adv. Materials* 2004, **16**, 1685–1706.
21. Petryayeva E.; Krull, U.J. Localized surface plasmon resonance: Nanostructures, bioassays and biosensing—a review. *Anal. Chimica Acta* 2011, **706**, 8–24.
22. Firstov, S.V.; Khegai, A.M.; Kharakhordin, A.V.; Alyshev, S.V.; Firstova, E.G.; Ososkov, Y.J.; Melkumov, M.A.; Iskhakova, L.D.; Evlampieva, E.B.; Lobanov, A.S.; Yashkov, M.V.; Gurynov, A.N. Compact and efficient o-band bismuth-doped phosphosilicate fiber amplifier for fiber-optic communications. *Sci. Reports* 2020, **10**, 1–9.
23. Vakhrushev, A.; Umnikov, A.; Lobanov, A.; Firstova, E.; Evlampieva, E.; Riumkin, K.; Alyshev, A.; Khegai, A.; Guryanov, A.; Iskhakova, L.; Melkumov, M.; Firstov, S. W-type and graded-index bismuth-doped fibers for efficient lasers and amplifiers operating in E-band. *Opt. Express* 2022, **30**, 1490–1498.
24. Khegai, A.; Alyshev, S.; Vakhrushev, A.; Riumkin, K.; Umnikov, A.; Firstov, S. Recent advances in Bi-doped silica-based optical fibers: A short review. *J. Non-Crystalline Solids: X* 2022, **16**, 100126.
25. Hernandez, M.A.V.; Martinez Gámez, M.A.; Martínez, J.L.L.; Kir'yanov, A.V. Enhanced near-infrared emission from holmium-ytterbium co-doped phosphate glasses containing silver nanoparticles. *Appl. Spectrosc.* 2014, **68**, 1247–1253.
26. Vallejo Hernandez, M.; Martinez Gámez, M.A.; Kir'yanov, A.; Martinez, J. Optical properties of phosphate glasses co-doped with Yb^{3+} and silver nanoparticles. *Chin. Phys. B* 2014, **23**, 124214.
27. Vijayakumar, R.; Nagaraj, R.; Suthanthirakumar, P.; Karthikeyan, P.; Marimuthu, K. Silver (Ag) nanoparticles enhanced luminescence properties of Dy^{3+} ions in borotellurite glasses for white light applications. *Spectrochimica Acta Part A: Mol. Biomol. Spectrosc.* 2018, **204**, 537–547.
28. Vijayakumar R.; Marimuthu, K. Luminescence studies on Ag nanoparticles embedded Eu^{3+} doped borophosphate glasses. *J. Alloy. Compd.* 2016, **665**, 294–303.
29. Bae, C.-H.; Lim, K.-S. Enhanced visible emission in Eu^{3+} doped glass containing Ag-clusters, Ag nanoparticles, and ZnO nanocrystals. *J. Alloy. Compd.* 2019, **793**, 410–417.
30. Pan, Z.; Ueda, A.; Aga Jr R.; Burger, A.; Mu, R.; Morgan, S. Spectroscopic studies of Er^{3+} doped Ge-Ga-S glass containing silver nanoparticles. *J. Non -Crystal. Solids* 2010, **356**, 1097–1101.
31. Cheng, P.; Zhou, Y.; Su, X.E.; Zhou, M.; Zhou, Z. The near-infrared band luminescence in silver NPs embedded tellurite glass doped with $Er^{3+}/Tm^{3+}/Yb^{3+}$ ions. *J. Alloy. Compd.* 2017, **714**, 370–380.
32. Zhao, G.; Xu, L.; Meng, S.; Du, C.; Hou, J.; Liu, Y.; Guo, Y.; Fang, Y.; Liao, M.; Zou, J.; Hu, L. Facile preparation of plasmon enhanced near-infrared photoluminescence of Er^{3+} doped Bi2O3-B2O3-SiO2 glass for optical fiber amplifier. *J. Lumin.* 2019, **206**, 164–168.
33. Swetha, B.; Keshavamurthy, K.; Jagannath, G. Influence of size of ag np on spectroscopic performances of Eu^{3+} ions in sodium borate glass host. *Optik* 2021, **240**, 166918.
34. Kindrat, I.I.; Padlyak, B.V.; Lisiecki, R.; Drzewiecki, A.; Adamiv, V.T. Effect of silver co-doping on luminescence of the Pr^{3+}-doped lithium tetraborate glass, *J. Lumin.* 2022, **241**, 118468.
35. Dan, H.K.; Trung, N.D.; Tam, N.M.; Ha, L.T.; Lien, T.K.; Thai, N.L.; Zhou, D.; Qiu, J. The effect of Al^{3+} ions on the self-reduction process of Yb^{3+} to Yb^{2+} ions and optical properties of Nd^{3+}/Yb^{n+} (n = 3, 2) co-doped

 doi:10.20944/preprints202410.0458.v1

transparent silicate glass-ceramics containing Ba_2LaF_7 nanocrystals and Ag nanoparticles. *Ceram. Int.* 2024, **50**, 25412-25421.

36. I. A. Bufetov, M. A. Melkumov, S. V. Firstov, K. E. Riumkin, A. V. Shubin, V. F. Khopin, A. N. Guryanov, and E. M. Dianov, "Bi-doped optical fibers and fiber lasers," *IEEE J. Select. Topics Quant. Electron.* **20**, 0903815 (2014).
37. Dianov, E.; Melkumov, M.; Firstov, S. Bismuth-doped fibre lasers and optical amplifiers. In *Handbook of Laser Technology and Applications,* (CRC Press, 2021), pp. 535–556.
38. Khonthon, S.; Morimoto, S.; Arai, Y.; Ohishi, Y. Redox equilibrium and NIR luminescence of Bi2O3-containing glasses. *Opt. Mater.* **31**, 2009, 1262–1268.
39. Peng, M.; Zollfrank, C.; Wondraczek, L. Origin of broad NIR photoluminescence in bismuthate glass and Bi-doped glasses at room temperature. *J. Phys.: Condens. Matter* 2009, **21** 285106.
40. Singh S.P.; Karmakar, B. Single-step synthesis and surface plasmons of bismuth-coated spherical to hexagonal silver nanoparticles in dichroic Ag: bismuth glass nanocomposites. Plasmonics 2011, **6**: 457–467.
41. Kir'yanov, A.V.; Halder, A.; Barmenkov, Y.O.; Das, S.; Dhar, A.; Bhadra, S.K.; Koltashev, V.V.; Plotnichenko, V.G.; Paul, M.C. Distribution of Bismuth and Bismuth-related centers in core area of Y-Al-SiO_2:Bi fibers. *J. Lightwave Technol.* 2015, **33**, 3649-3659.
42. Halder, A.; Kir'yanov, A.; Barmenkov, Y.; Sekiya, E.H.; Saito, K. Discussion on Raleigh scattering as a dominant loss factor in VIS/NIR in bismuth-doped silicate fibers [invited]. *Opt. Mater. Express* 2019, **9**, 2817–2827.
43. Krishnan, M.L.; Neethish, M.; Kumar, V.R.K.; Vendamani, V.; Devi, K.D.; Mohan, D.B.; Nandhagopal, P.; Behera, N. Photoluminescence & structural studies of Ag: Alkali bismuth silicate glasses. *Optik* 2023, **273**, 170474.
44. Zhu, H.; He, Z.; Wang, J.; Zhang, W.; Pei, C.; Ma, R.; Zhang, J.; Wei, J.; Liu, W. Microcavity complex lasers: from order to disorder. *Ann. der Physik* 2024, **536**, 2400112.